Morphological Development at the Interface of Polymer/Polymer Bilayer with an in-Situ Compatibilizer under Electric Field

Dong Han Kho, Seung Hun Chae, Unyong Jeong, Hwang Yong Kim, and Jin Kon Kim*

National Creative Research Initiative Center for Block Copolymer Self-Assembly, Department of Chemical Engineering and Polymer Research Institute, Division of Electrical and Computer Engineering, Pohang University of Science & Technology, Kyungbuk 790-784, Korea

Received March 2, 2004; Revised Manuscript Received February 27, 2005

ABSTRACT: An electric field was applied to reactive bilayer thin films consisting of poly(methyl methacrylate-*ran*-glycidyl methacrylate) (PMMA−GMA) and polystyrene (PS) with various amounts of monocarboxylic acid end-functionalized PS (PS-mCOOH). The fast growing wavelength (λ_{max}) of the interfacial fluctuation under an electric field decreased sharply and approached a steady value with increasing amounts of PS-mCOOH. This is because of the decrease in interfacial tension (γ) between PMMA−GMA and PS resulting from the formation of PMMA-*g*-PS copolymers in-situ from the reaction between two functional groups of GMA and mCOOH. The reduction of γ with increasing amount of PS-mCOOH was verified from a reduction in the dispersed domain size. For a reactive bilayer where Y-shaped graft copolymers were formed, the pillars with flattened top surface were observed even when they did not touch the upper electrode. This result is in contrast to that seen for nonreactive bilayer or even other reactive bilayer where diblock copolymers were generated. Also, the maximum pillar height obtained for the reactive bilayer generating graft copolymers was smaller than that for nonreactive bilayer as well as other reactive bilayer generating diblock copolymers. The mechanism of the growth of the pillars of the reactive bilayer was discussed in terms of the chain architecture of copolymers formed in-situ at the interface.

I. Introduction

The electrohydrodynamic instabilities of thin liquid films have been extensively investigated theoretically[1−3] and experimentally.[4−7] Instability of the interface between two immiscible polymeric liquids or the surface in air/polymeric liquid occurs when the applied electric field (E-field) exceeds a threshold value at which the E-field dominates over the interfacial energy difference between the two liquids or the surface tension for air/polymer system. In this situation, one of the components forms cylindrical pillars as long as the dielectric constants (ϵ) and interfacial (surface) tension between the two components are not the same. E-fields have also aligned microdomains in block copolymers along the E-field direction because of the different values of ϵ for block components.[8−11]

Schäffer et al.[12,13] investigated the electrohydrodynamic instability of a thin layer of a highly viscous polymer in the presence of an air gap. Lin et al.[14−17] extended the study of interfacial instability to polymer/polymer bilayer films under an E-field and showed that the fastest growing wavelength (λ_{max}) for bilayer films under E-field is given by

$$\lambda_{max} = 2\pi/q_{max} = 2\pi\sqrt{\frac{\gamma U(\epsilon_1\epsilon_2)^{1/2}}{\epsilon_0(\epsilon_2-\epsilon_1)^2}}(E_1E_2)^{-3/4} \propto \gamma^{1/2}h^{3/2}/U(\Delta\epsilon) \quad (1)$$

where γ is the interfacial tension between the components, U is the applied voltage, ϵ_i and E_i are the dielectric constant and the electric field of component i, respectively, ϵ_0 is the permittivity in a vacuum, and h is the overall film thickness. λ_{max} characterizes the center-to-center distance of pillars ($\langle d\rangle$).

For a single layer film, γ in eq 1 becomes the surface tension. Since the surface tension is much larger than the interfacial tension, λ_{max} (or $\langle d\rangle$) obtained from the bilayer polymer films was smaller than that obtained from the single layer polymer film at given h. For instance, $\langle d\rangle$ is 47.4 μm for polyisoprene (PI) single layer, which is about twice than that (20.6 μm) for PI/oligomeric dimethylsiloxane bilayer.[14] This value was further reduced 4.0 μm when polystyrene/poly(methyl methacrylate) (PS/PMMA) bilayer was used.[15]

However, it is better to obtain a smaller diameter or $\langle d\rangle$ of pillars for the purpose of nanoscale patterning. According to eq 1, at a given film thickness λ_{max} becomes smaller with decreasing γ and increasing U, but U cannot be increased indefinitely because of dielectric breakdown at very high U.[18] Thus, an effective means to decrease $\langle d\rangle$ is to reduce γ, which can be achieved by the addition of block (or graft) copolymers or in-situ formed block (or graft) copolymers by the reaction at the interface.[19−21] However, when a block copolymer is added to one layer, all the block copolymer chains do not move to the interface due to the micelle formation. Furthermore, when a block copolymer film prepared by the floating method is sandwiched between two polymer layers, it is hard to achieve a flat interface in the lateral direction.

In this study, we employed an in-situ reactive polymer bilayer under an E-field to decrease γ. The reactive bilayer consists of poly(methyl methacrylate-*ran*-glycidyl methacrylate) (PMMA−GMA) and a mixture of PS and monocarboxylic acid end-functionalized PS (PS-mCOOH). The λ_{max} for a reactive bilayer decreased sharply and approached a steady value with increasing

* To whom correspondence should be addressed: e-mail jkkim@postech.ac.kr.

10.1021/ma0495846 CCC: $30.25
Published on Web 04/05/2005

Table 1. Molecular Characteristics of Polymers Used in This Study

	M_n	M_w/M_n	η^* (Pa·s) at 180 °C	T_g (°C)	ϵ	no. of functional groups per chain[e]
PMMA-GMA	28 800[a]	1.51[a]	6100	105	3.6[c]	2.0
PS	23 000[b]	1.06[b]	120		2.5[c]	0
PS-mCOOH	41 000[b]	1.11[b]	260	100	2.5[c]	1
PDMS					2.98[d]	

[a] Determined by gel permeation chromatography(GPC) with PMMA standards. [b] Determined by gel permeation chromatography(GPC) with PS standards. [c] From ref 13. [d] From ref 35. [e] Determined by a 500 MHz proton nuclear magnetic spectroscope (^{1}H NMR; DRX 500, Bruker).

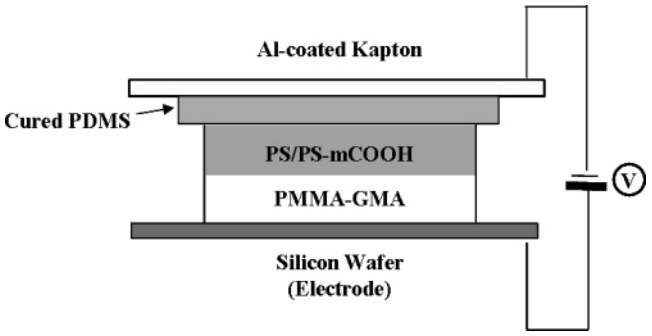

Figure 1. Schematic of E-field used in this experiment. The reactive bilayer is confined by two electrodes, Al-coated Kapton (upper electrode) and a silicon wafer (lower electrode). To eliminate a possible air trap, cured PDMS layer was employed.

amounts of PS-mCOOH. This is because of the decrease in γ resulting from the formation of PMMA-*g*-PS copolymers at the interface due to the reaction between GMA and COOH at high temperatures.[22−25]

II. Experimental Section

PS and PS-mCOOH were anionically synthesized in this laboratory, and PMMA-GMA was synthesized by free-radical polymerization.[23,24] Molecular characteristics of the polymers employed in this study are summarized in Table 1. A schematic of applying an E-field to bilayer thin films is given in Figure 1. A thin film of PMMA−GMA was spin-coated from a toluene solution onto a silicon wafer that was first treated by piranha solution (70/30 v/v of H_2SO_4/H_2O_2) for 30 min at 90 °C and dried thoroughly by fresh N_2 gas. Then, a thin layer of PS with various amounts of PS-COOH on the top of PMMA-GMA film was spin-coated from a mixed solvent of cyclohexane/toluene (87/13 v/v). When cyclohexane itself was used for the solvent of PS/PS-mCOOH, the top of the PS film was not smooth, as pointed out by Macosko and co-workers.[26] It is noted that the mixed solvent of cyclohexane/toluene did not dissolve the PMMA layer. The thickness of the PMMA-GMA layer and the bilayer was 250 and 500 nm, respectively, determined by a spectroscopic ellipsometer (J.A. Woollam Co.; M-2000V) at room temperature.

The silicone wafer and an aluminum-coated Kapton sheet with a thickness of 51 μm (Sheldahl Co.) were used as lower and upper electrodes, respectively. Since the surface of Kapton film is not very smooth, a very tight contact between the Kapton sheet and PS layer was impossible due to the formation of an air trap between these two. This air trap was completely removed by spin-coating a mixture of 90/10 (w/w) poly(dimethylsiloxane) (PDMS) and curing agent (SYLGARD 184, Dow Corning) onto the Kapton sheet and cross-linking at 80 °C for 12 h under vacuum. The thickness of cured PDMS was 40 μm, and 2000 V was applied to the entire film thickness. The voltage applied for the bilayer (PMMA-GMA/PS-COOH) was obtained:

$$U_{\text{bilayer}} = \frac{\epsilon_1\epsilon_2 h_3 + \epsilon_1\epsilon_3 h_2}{\epsilon_1\epsilon_2 h_3 + \epsilon_1\epsilon_3 h_2 + \epsilon_2\epsilon_3 h_1} U_{\text{total}} \qquad (2)$$

where h_1 (ϵ_1), h_2 (ϵ_2), and h_3 (ϵ_3) are the film thicknesses (and dielectric constants) of cured PDMS layer (1), PS layer (2), and PMMA layer (3), respectively. From the values in Table 1, a voltage of 25 V was applied to the bilayer film.

The bilayer was reacted at 180 °C under a N_2 atmosphere for various times in the presence of an E-field and quenched to room temperature before the E-field was removed. Finally, the Kapton film as well as the cured PDMS layer was carefully peeled off from the bilayer. The morphological development of the bilayer at the interface was investigated by tapping mode atomic force microscopy (AFM: a Digital Instrument D3000) with silicone nitride tips on cantilevers (Nanoprobe) and a spring constant ranging from 40.0−66.0 N/m and field emission scanning electron microscopy (FE-SEM: Hitachi S-4200). For all these experiments, the PS (and unreacted PS-mCOOH) phase in the bilayer was selectively etched out by cyclohexane for 3 h at room temperature, and the solvent was completely removed under vacuum at room temperature for 5 h.

The cross-sectional morphology of the bilayer was examined by transmission electron microscopy (TEM Hitachi 7600) on operating at 120 kV. The sample preparation was as follows. A thin layer of carbon was first evaporated onto the PS-mCOOH/PMMA-GMA bilayer film, covered with an epoxy (Araldite 502 embedding kit, Polysciences, Inc.), and cured at room temperature for 12 h and at 60 °C for 24 h. The epoxy/carbon/(PS-mCOOH/PMMA-GMA) film was peeled off from the silicone wafer after being immersed in liquid nitrogen. A carbon layer was again evaporated onto the other side of PS-mCOOH/PMMA-GMA, covered with epoxy, and cured. Thin sections (less than 100 nm) from epoxy/carbon/(PS-mCOOH/PMMA-GMA)/carbon/epoxy were obtained by using an Ultramicrotome (RMC MT-7000) with a diamond knife and stained by ruthenium tetraoxide (RuO_4). The PS phase appeared dark in TEM images because of selective staining of RuO_4.

III. Results

Figure 2 gives AFM height images of the PMMA-GMA phase generated from a PS/PMMA-GMA bilayer exposed to a 25 V at 180 °C for various times. All of these AFM images were obtained after the upper PS layer was selectively removed by using a cyclohexane. Before an E-field was applied, the amplitude of the fluctuations was too small to observe. At 1 h exposure of the E-field, fluctuations having a well-defined lateral wavelength appeared due to a ring pattern in the 2D fast Fourier Transform (FFT), as shown Figure 2b. It is known that $\lambda_{\max}$ in initial fluctuation determines the final distance ($\langle d \rangle$) corresponding to the center-to-center spacing between two neighboring pillars.[14] As the exposure time was increased, the amplitude of the fluctuations increased, and the fluctuations became sharper and more well-defined (Figure 2c). At a long exposure time (~24 h), the pillars made of PMMA-GMA touched the cured PDMS layer (Figure 2d), from which the diameter of the pillars and $\langle d \rangle$ were 2.9 ± 0.2 and 4.7 ± 0.3 μm, respectively. The insets in Figure 2b−d represent 2D FFT of AFM images. From the scattering vector corresponding to the maximum intensity, q^*, the $\lambda_{\max}$ between PMMA-GMA pillars was calculated ($2\pi/q^*$) to be 4.70 μm. We found that $\lambda_{\max}$ obtained from FE-SEM images (not shown here) is essentially the same as that

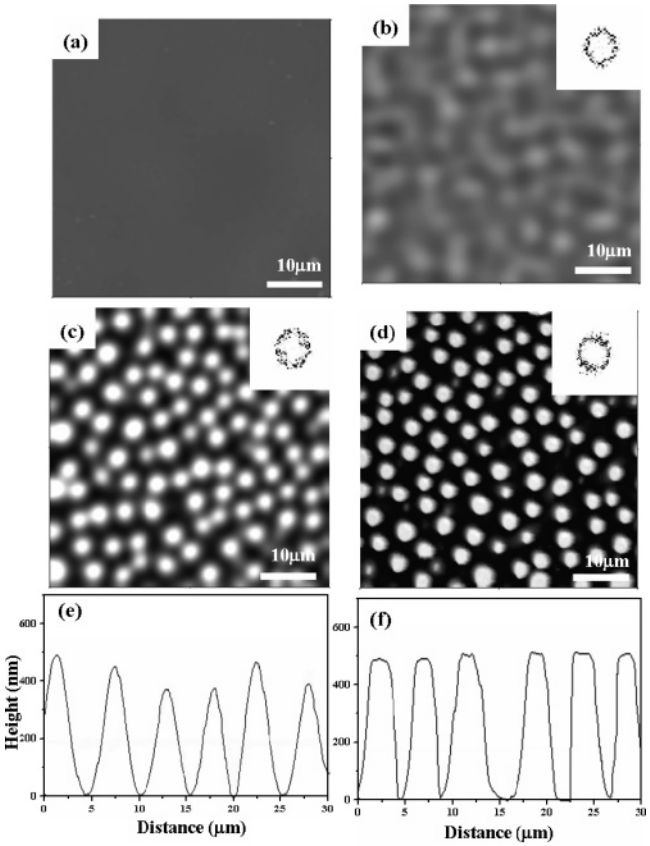

Figure 2. AFM height images (inset: 2D FFT) of the PMMA-GMA phase exposed to 25 V at 180 °C for various times: (a) before E-field, (b) 1 h, (c) 12 h, and (d) 24 h. (e) and (f) are height profiles of AFM images of (c) and (d), respectively. PS phase was etched out by a selective solvent of cyclohexane.

obtained from AFM. It is noted that the AFM height image of the top surface of the PS film in PS/PMMA-GMA bilayer without etching out PS layer did not show any discernible fluctuation. This indicates that the cured PDMS layer plays a role as a solid layer, as evident from the fact that the complex viscosity of cured PDMS (η^*_{PDMS}) at 180 °C was 1.0×10^6 Pa·s, which is much larger than $\eta^*_{PS} = 120$ Pa·s and $\eta^*_{PMMA-GMA} = 6100$ Pa·s.

AFM height images for a reactive bilayer consisting of PS with various amounts of PS-mCOOH and PMMA-GMA after being exposed to 25 V at 180 °C for 24 h are given in Figure 3. The PS (and unreacted PS-COOH) parts were etched out by cyclohexane. It is seen that with increasing the amount of PS-mCOOH in the PS layer, the diameter (D) of the PMMA-GMA pillars as well as $\langle d \rangle$ decreased. Previously, we reported that for PS-mCOOH/PMMA-GMA bilayer with 600 μm thickness, the initial flat interface roughens and the root-mean-square (rms) of the roughness reaches as large as ~180 nm when reacted at 180 °C for 24 h without an E-field.[27] However, cylindrical pillars with well-defined size were not observed.

From the results given in Figure 3, plots of λ_{max} vs amount of PS-mCOOH in PS layer are shown in Figure 4. With increasing amount of PS-mCOOH, λ_{max} sharply decreased at small amounts and approached a steady value at higher amounts. The values of D and $\langle d \rangle$ for 100% PS-mCOOH/PMMA-GMA bilayer film were 0.88 $\pm$ 0.1 μm and 1.05 $\pm$ 0.2 μm, respectively, which is about a quarter of the D (2.9 $\pm$ 0.2 μm) and $\langle d \rangle$ (4.70 $\pm$ 0.3 μm) of the nonreactive bilayer (PS/PMMA-GMA). The

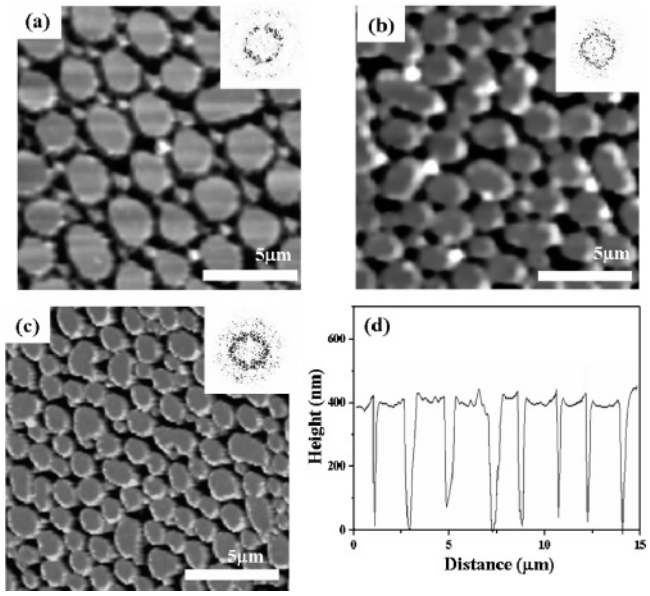

Figure 3. AFM height images and 2D FFT (inset) of the PMMA-GMA pillars in PS with various amounts of PS-mCOOH and PMMA−GMA bilayer exposed to 25 V at 180 °C for 24 h. The amount of PS-mCOOH in PS layer was (a) 5, (b) 10, and (c) 100 wt %. (d) Height profiles of AFM image of (c).

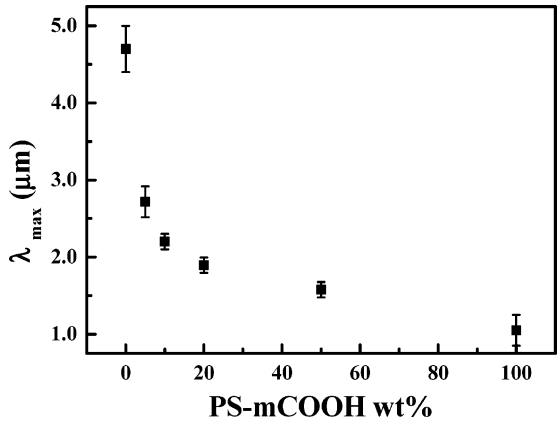

Figure 4. Change of λ_{max} with the amount of PS-mCOOH for (PS + PS-mCOOH)/PMMA-GMA bilayer exposed to an E-field.

reduced $\langle d \rangle$ with increasing amount of PS-mCOOH implies a decrease in interfacial tension between PS and PMMA-GMA ($\gamma_{(PS+PS-mCOOH)/PMMA-GMA}$). It is well-known that the graft copolymers formed in-situ from the reaction between two functional groups of COOH and GMA act as an effective compatibilizer between immiscible PS and PMMA-GMA layer. Once the graft copolymers are located between PS and PMMA-GMA layers, the interfacial tension decreases.

Since $\lambda_{max} \propto \gamma^{1/2}$ from eq 1, we can obtain $\gamma_{(PS+PS-mCOOH)/PMMA-GMA}$ from Figure 4. Although γ for a reactive blend can be measured by the Neumann triangle method (NT),[28] it is very difficult to measure $\gamma_{(PS+PS-mCOOH)/PMMA-GMA}$. This is because of the difficulty in the choice of the third component for NT due to a small value of $\gamma_{PS/PMMA}$ without PS-mCOOH (~1.2 mN/m).[15] Thus, we tried to measure $\gamma_{(PS+PS-mCOOH)/PMMA-GMA}$ from the change of the dispersed domain size (D_s) in the PS with various amounts of PS-mCOOH and PMMA-GMA blend because $\gamma \propto D_s$.[29,30] Of course, in this situation, the coalescence between the dispersed domains should be minimized, which is usually met for

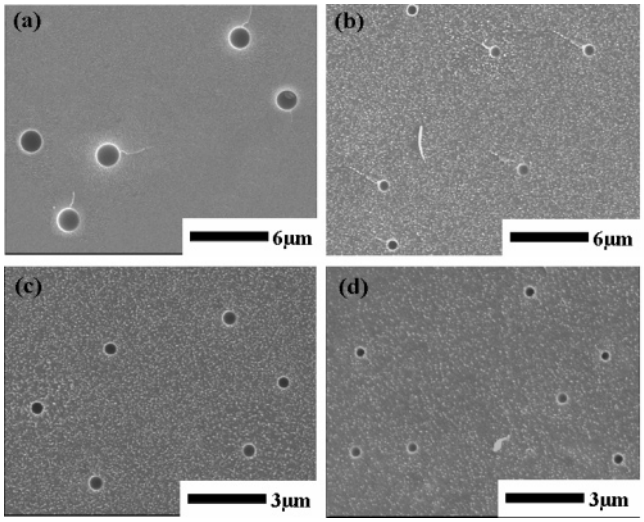

Figure 5. SEM images of 99/1 (w/w) (PS + PS-mCOOH)/PMMA-GMA blend prepared by melt mixing with Minimax molder. The amount of PS-mCOOH in PS phase was (a) 0, (b) 2, (c) 5, and (d) 25 wt %.

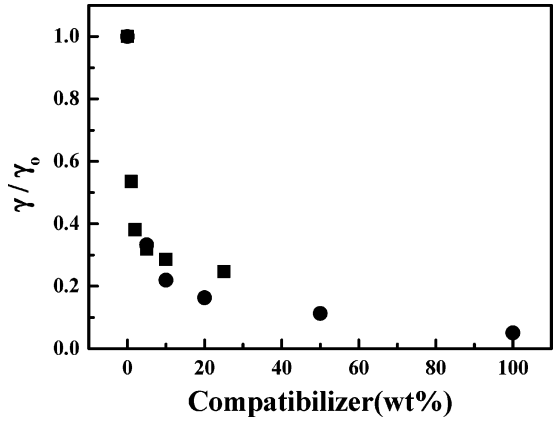

Figure 6. Plot γ/γ_0 vs weight fraction of PS-mCOOH in PS + PS-mCOOH and PMMA system measured by the reduced domain size (■) and the reduced λ_{max} (●).

the very small amounts of the dispersed phase (less than ~1 wt %).

Figure 5 shows FE-SEM images of dispersed PMMA-GMA domains in 99/1 (w/w) PS with various amounts of PS-mCOOH and PMMA-GMA blends prepared at 220 °C for 20 min by using a Minimax molder (Bau Technology, BA-915) under a nitrogen atmosphere. The dispersed PMMA-GMA domains were selectively etched out by acetic acid for 6 h. Each SEM image contained 5−7 domains with uniform-sized and well-defined circles. Since coalescence between PMMA domains was effectively prevented, γ is directly proportional to D_s. To obtain dispersed domain size accurately, 10 frames of SEM images were employed at each amount of PS-mCOOH because of a few disperse domains at each SEM image.

Figure 6 gives the reduction in the interfacial tension, γ/γ_0, with the amount of PS-mCOOH estimated from both D/D_0 and $\lambda_{max}/\lambda_{max,0}$. Here, the subscript "0" stands for PS/PMMA-GMA without PS-mCOOH. It is seen that γ/γ_0 obtained from both data are in good agreement; thus, eq 1 can be used to obtain γ of a reactive blend. γ decreased very sharply at lower amounts of PS-mCOOH and approached a steady value at higher amounts. This behavior has been known as compatibilization (or emulsification) effect for reactive blends.[31]

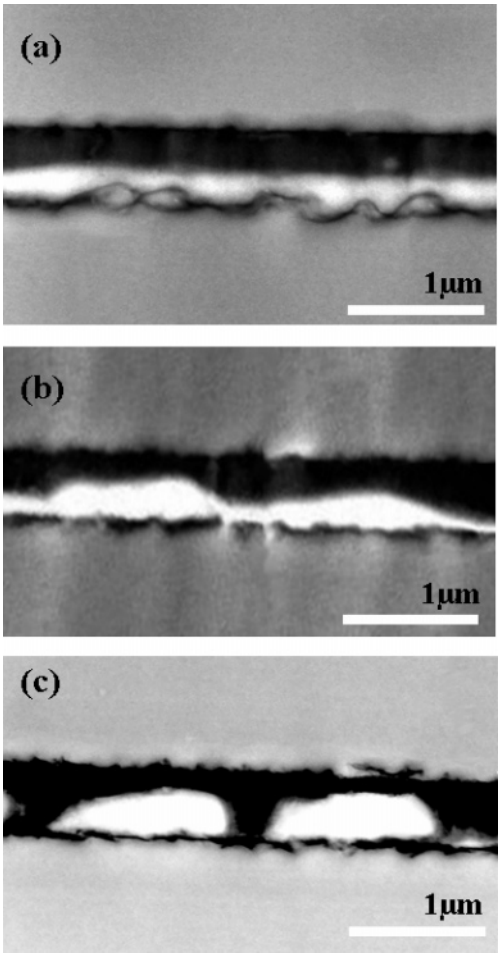

Figure 7. Cross-sectional TEM image of PS-mCOOH/PMMA-GMA bilayer film exposed to 25 V at 180 °C for various times: (a) before E-field, (b) 6 h, and (c) 24 h.

Now, we consider in detail the morphological development of a reactive bilayer under an E-field. As shown in Figure 3, the PMMA-GMA pillars in a reactive bilayer do not touch the top of the PS layer, although the $\langle d \rangle$ decreases compared with nonreactive bilayer. Furthermore, because the PS layer was etched out, the detailed morphology of the bilayer through the entire film thickness cannot be investigated. Figure 7 gives cross-sectional TEM images of 100% PS-mCOOH/PMMA-GMA bilayer exposed to a 25 V at 180 °C for various times. The dark area represents PS-mCOOH phases which are selectively stained by RuO_4.

Before applying of the E-field, the interface between PS-mCOOH and PMMA-GMA is very flat. With increasing exposure time, the generation of PMMA-GMA pillars is clearly seen (Figure 7b). However, the PMMA-GMA pillars do not touch the cured PDMS layer even at a longer exposure time (24 h), and thus the height of PMMA-GMA pillars is smaller than that of nonreactive bilayer, as shown in AFM images (Figure 3). The diameters of pillars and center-to-center distance between two neighboring pillars are 0.88 and 1.02 μm, respectively, which is consistent with AFM images (Figure 3d) and FE-SEM images (not shown)). Furthermore, the pillars generated from the reactive bilayer exhibited rather a flattened top surface even at 6 h where the pillars did not reach the final height (Figure 7b).

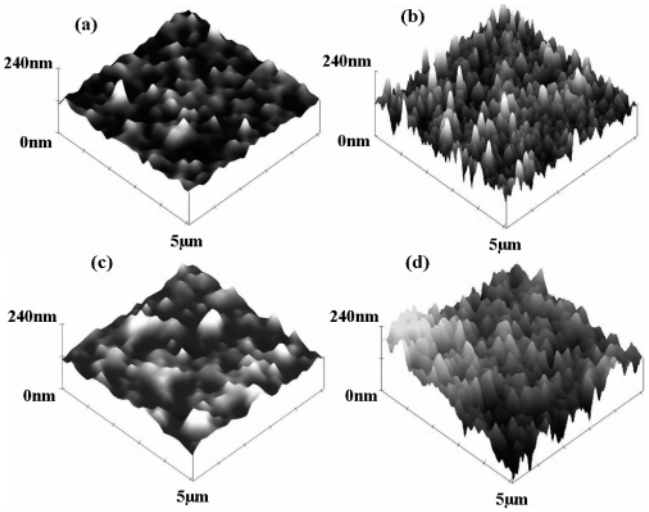

Figure 8. 3D AFM height images of the interfacial roughness without E-field for PS-mCOOH/PMMA-GMA bilayer film at two different temperatures and times: (a) 180 °C for 3 h, (b) 180 °C for 24 h, (c) 200 °C for 3 h, and (d) 200 °C for 24 h. PS phase was etched out by a selective solvent of cyclohexane.

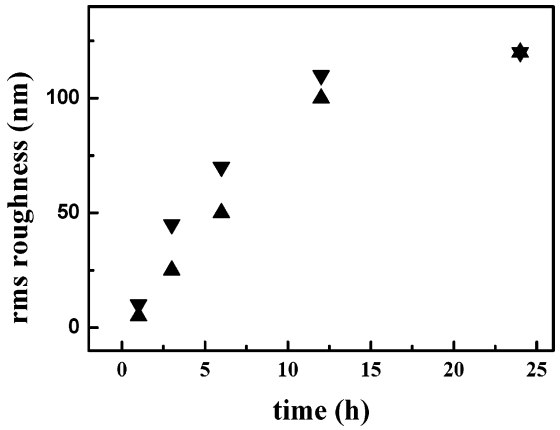

Figure 9. The rms roughness changes with time without E-field for PS-mCOOH/PMMA-GMA bilayer film at two different temperatures, 180 °C (▲) and 200 °C (▼).

IV. Discussion

Now we discuss why the development of the pillar for a reactive bilayer generating graft copolymers is different from that for a nonreactive bilayer. It is seen in Figure 7b that the pillars generated from the reactive bilayer forming graft copolymers exhibited rather a flattened top surface even though the pillars did not touch the cured PDMS layer, whereas those generated from nonreactive bilayer showed characteristics of sinusoidal fluctuations and touched the cured PDMS layer (see Figure 2c,e).

We investigated the interfacial morphology for a bilayer forming graft copolymers without E-field. Figure 8 gives AFM height images for the bilayer reacted at two different temperatures (180 and 200 °C) for different times (3 and 24 h). It is noted that the viscosities of PS-mCOOH and PMMA-GMA at 200 °C are a quarter of those at 180 °C. As shown in Figure 8, the rms roughness of the interface increased with time even under the absence of an E-field. Similar roughness change for a reactive blend was also reported previously.[27] Time evolution of the rms roughness at two temperatures is given in Figure 9. Although the increase in the rms roughness at 200 °C was faster than at 180 °C at short reaction times due to enhanced mobility, the

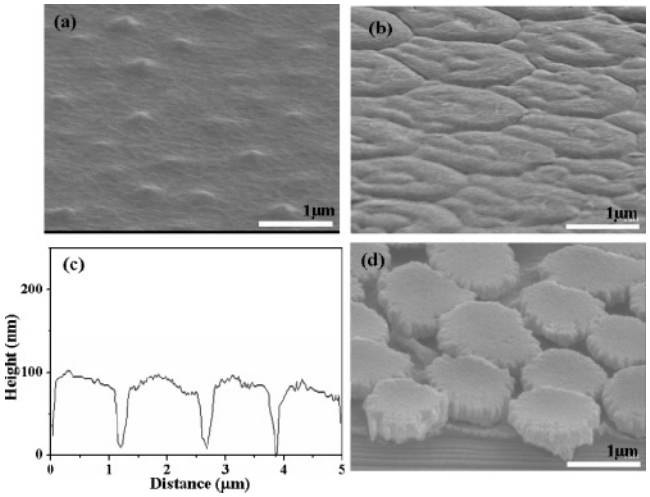

Figure 10. SEM images of the formation of PMMA pillars at various reaction times at 180 °C for PS-mCOOH/PMMA-GMA bilayer: (a) 1, (b) 3, and (d) 24 h. (c) Cross-sectional height profile of the pillars from AFM image (not shown) reacted for 3 h.

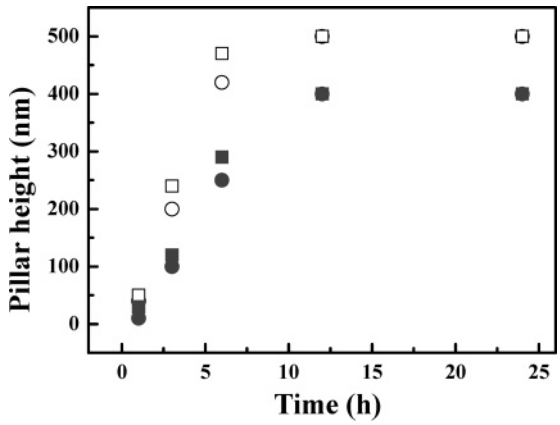

Figure 11. Height change of PMMA-GMA pillar with time under 25 V at two temperatures (180 °C (○, ●) and 200 °C (□, ■)) for PS/PMMA-GMA nonreactive bilayer (open symbols) and for PS-mCOOH/PMMA-GMA reactive bilayer (closed symbols).

leveled-off value (~120 nm) was the same at both temperatures. This is because sufficient amounts of graft copolymers were in-situ formed at the interface at longer reaction times at both temperatures. The wavelength of the roughness formed by the reaction alone, though not well-defined, is ~170 nm.

Figure 10 gives the FE-SEM images at three different reaction times for the reactive bilayer forming graft copolymers under the E-field. The interfacial shape of the bilayer reacted for 1 h shows the characteristic sinusoidal fluctuation (Figure 10a) similar to a nonreactive bilayer. For 3 h reaction, distinct pillars with $\langle d \rangle \sim 1\ \mu$m are clearly seen. This $\langle d \rangle$ is much larger than the wavelength (~170 nm) of the roughness formed without E-field. Interestingly, flat pillars were observed even though the pillar height was just ~100 nm, as demonstrated in the SEM image (Figure 10b) and the height profile (Figure 10c) of AFM image (not shown), which was distinctly different from nonreactive bilayer. With increasing reaction time, the height of pillars increased more, even though the growth rate of the pillar height is slower than that for the nonreactive bilayer. However, the pillar did not touch the cured PDMS layer (Figure 10d).

Figure 11 gives the change of the pillar height with time under an E-field for nonreactive and reactive

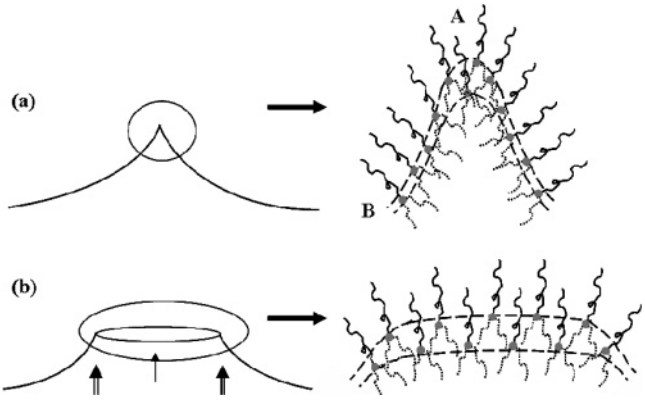

Figure 12. Schematic of the interfacial shape for the reactive bilayer generating graft copolymers. (a) A sharp interface for Y-shaped graft copolymers, where the interfacial thickness given by two dashed lines near the E-field induced-divergent point (A) is larger than that far from the divergent point (B). (b) A flat interface for Y-shaped graft copolymers.

bilayers. It is seen that the growth rate of the pillar height for the reactive bilayer was slower than that for the nonreactive bilayer because of the presence of in-situ formed graft copolymers at the interface. Also, the growth rate of the pillars in the reactive bilayer increases with increasing reaction temperature due to enhanced mobility.

The flat pillar as shown in Figure 10b,c could be related to the formation of Y-shaped PMMA-*g*-PS copolymers at the interface, where two (or more) arms were PMMA chains. The interfacial thickness of graft copolymers was larger than that of block copolymers.[27,34] This is because the two arms of the PMMA chains in the PMMA-*g*-PS copolymers need more area to avoid the steric hindrance. During early reaction times less than ~1 h, a sharp (or divergent) interface could maintain because the amount of graft copolymers in-situ formed at the interface was not much. But, with increasing the reaction time, the interfacial thickness became larger due to the larger amounts of in-situ formed graft copolymers, and the interfacial strength became stronger. Electric-field-induced divergent points (site A in Figure 12a) would contain larger amounts of the graft copolymer and stronger interfacial strength than other points (say, site B in Figure 12a) because of larger interfacial area generation near site A by E-field. Thus, the further growth of pillars near site A would be hampered. Also, the steric hindrance between the PMMA chains near site A would be very severe because PMMA-GMA two arms are located inside sharp interface, as shown in Figure 12a. Thus, a broad interface would be more stable than a sharp interface for graft copolymers, as shown in Figure 12b.

To check whether the chain architecture of copolymers formed in-situ significantly affects the growth mechanism of pillars, we prepared another reactive bilayer consisting of mono-GMA end-functionalized PS (M_w of 50 100) and monocarboxylic acid end-functionalized PMMA (M_w of 30 200) reacted at 180 °C for 24 h under E-field. In this reactive bilayer, diblock copolymers were formed at the interface. At short reaction times, the pillar development was a characteristic of a sinusoidal wave (Figure 13a). Figure 13b,c gives SEM images and height profiles of pillars from AFM image (not shown) reacted at 6 h, where some pillars located at site A began to touch the cured PDMS layer. Interestingly, these pillars maintained a sharp (or divergent) interface.

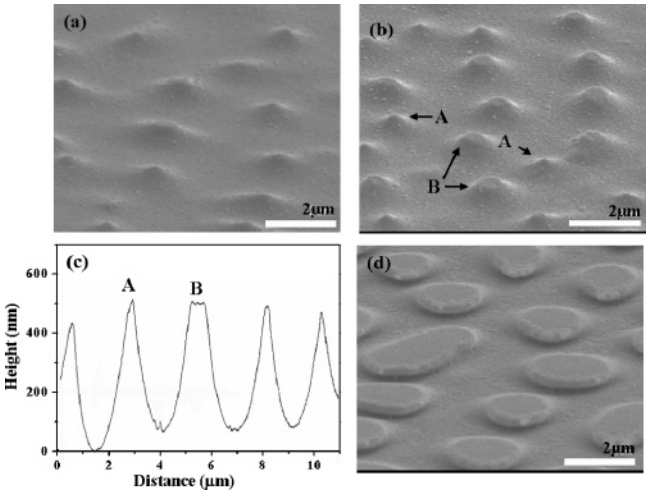

Figure 13. SEM images of the formation of PMMA pillars at various reaction times for PS-GMA/PMMA-mCOOH bilayer where PS−PMMA diblock copolymers were formed near the interface: (a) 1, (b) 6, and (d) 24 h. (c) Cross-sectional height profile of pillars from AFM image (not shown) reacted for 6 h, showing two different morphologies. Pillars at sites A and B represent before and after touching the cured PDMS layer.

Other pillars located at site B become flat at the top due to the flowing of PMMA-COOH pillars after touching the cured PDMS layer. Finally, at 24 h reaction times, all PMMA-COOH pillars touched the cured PDMS layer and have flat top surface (Figure 13d). We found that $\langle d \rangle$ of this reactive bilayer was 3.7 ± 0.1 μm, which is smaller than that of nonreactive bilayer (4.7 ± 0.3 μm). Therefore, the growth mechanism of pillars for this reactive bilayer forming diblock copolymers is very similar to that for nonreactive bilayer. This is because of smaller interfacial thickness for diblock copolymers compared with that for graft copolymers.[34] The interfacial strength near the divergent point of the curvature would not be too strong to prevent further growth of pillars compared with that of pillars forming graft copolymers. Also, even if the PMMA chains are located inside a sharp interface, steric hindrance between PMMA chains of diblock copolymers would not be severe compared with graft copolymers. Thus, a sharp interface could maintain for the development of pillars containing diblock copolymers. On the basis of results shown in Figures 10, 12, and 13, we conclude that a flat top surface of pillars observed at earlier reaction times for the reactive bilayer employed in this study is mainly due to the formation of Y-shaped graft copolymers at the interface.

To check whether the flatness of pillars might be due to increased viscosity resulting from in-situ formed graft copolymer, we carried out an experiment of a nonreactive bilayer with higher molecular weights of PS and PMMA (190 000 and 100 000) whose viscosities at 180 °C (9900 and 181 000 Pa·s, respectively) are at least 30 times greater than those of PS-mCOOH and PMMA-GMA (240 and 6100 Pa·s, respectively) employed in this study. However, we found that the growth mechanism of PMMA pillar was essentially the same as that for nonreactive bilayer. In other words, a sinusoidal growth of pillars observed at earlier times became cylindrical pillar, and a flat pillar was observed after touching the electrode.

Also, it may be considered that the smaller pillar height obtained at 24 h in this study might be due to insufficient exposure time resulting from an increased

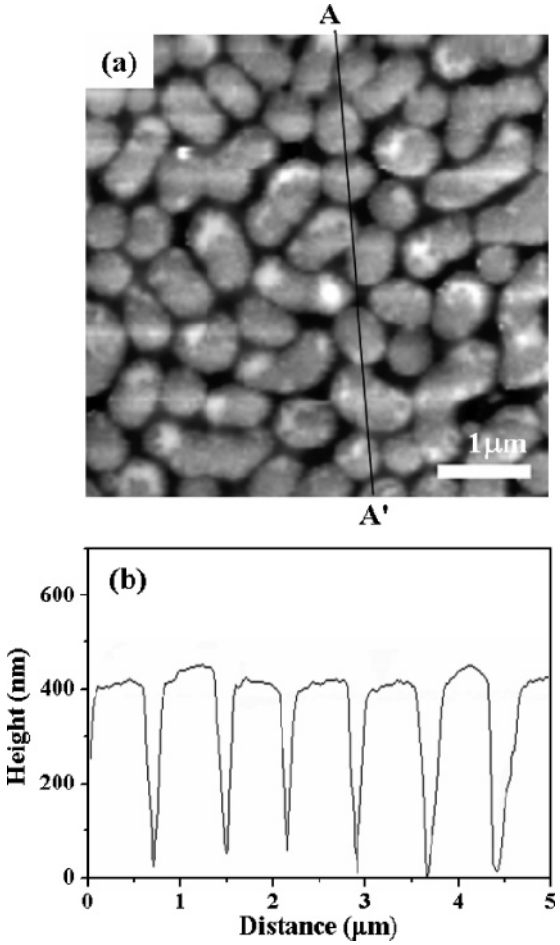

Figure 14. (a) AFM height image of the PMMA-GMA pillar for PS-mCOOH/PMMA-GMA bilayer film under 37 V at 180 °C for 24 h. (b) Cross-sectional height profile of the AFM image along the line (AA′).

viscosity (or reduced mobility) by the in-situ formed graft copolymers near the interface. The predicted characteristic relaxation time, τ_{max}, is given by[14]

$$\tau_{max} = \frac{3C(\eta)\gamma_{12}U^2\epsilon_1\epsilon_2}{(h_1h_2)^{3/2}\epsilon_0{}^2(\epsilon_2 - \epsilon_1)^4(E_1E_2)^3} \quad (3)$$

where $C(\eta)$ contains viscosities of PMMA-GMA and PS-mCOOH. The substitution of all parameters into eq 3 gives a τ_{max} of 7.2 s for the reactive bilayer employed in this study. This is, however, much smaller than the experimental data (1 h). We found that even when the reaction time was increased to 72 h at 180 °C for PS-mCOOH/PMMA-GMA reactive bilayer under a 25 V, the height of PMMA-GMA pillars was ∼400 nm, which is the same as the height reacted for 24 h. Also, the $\langle d \rangle$ was the same for both cases. Furthermore, the height of PMMA-GMA pillars and the $\langle d \rangle$ reacted at 200 °C for 24 h are essentially the same as those at 180 °C. This suggests that the pillar morphology reacted for 24 h at 180 °C is not an intermediate state, but a steady state.

We investigated whether the height of PMMA-GMA pillars in the reactive bilayer generating graft copolymers could be increased further with increasing E-field. Figure 14 shows the AFM height image and height profile of PMMA-GMA pillars for PMMA-GMA/PS-COOH bilayer exposed to 37 V at 180 °C for 24 h. The values of D and $\langle d \rangle$ of PMMA-GMA pillar were 0.55 ± 0.02 μm and 0.70 ± 0.03 μm, respectively. The decrease in $\langle d \rangle$ (or λ_{max}) from 1.05 ± 0.2 to 0.70 ± 0.03 μm with increasing U from 25 to 37 V/μm is consistent with the prediction by eq 1. Interestingly, the final pillar height at 37 V was ∼420 nm, slightly larger than that (∼400 nm) at 25 V, whereas the aspect ratio (D/H in which H is the pillar height) at 37 V was 0.76, distinctly larger than that (0.45) at 25 V. This indicated that larger interfacial areas were formed due to the increased interface instability generated by stronger electrostatic force compared with restoring surface tension and steric hindrance effect. But, the pillars did not touch the cured PDMS layer even at 37 V. Thus, the smaller height of pillars observed for the reactive bilayer generating Y-shaped graft copolymers compared with the nonreactive bilayer (or even another reactive bilayer generating diblock copolymers) might not be ascribed to insufficient E-field. However, it would be of interest to investigate whether the pillar heights for the reactive bilayer will touch the cured PDMS at a very high voltage (for instance, 100 V). This is a subject for future investigation.

For cylindrical pillars with hexagonal packing, the D is given by

$$D/\langle d \rangle = \left(\frac{2\sqrt{3}\phi}{\pi}\right)^{1/2} \quad (4)$$

where ϕ is the volume fraction of PMMA-GMA and given by H_0/H_{final}, in which H_0 is the original thickness (250 nm) of PMMA-GMA in the bilayer and H_{final} is the final height of PMMA-GMA pillar. Here, it is assumed that there is no pure PMMA-GMA layer below the bottom of pillars. Namely, all PMMA-GMA pillars touched the lower electrode, as verified by AFM image (see Figure 3d). For the pillars with $D/\langle d \rangle = 0.84$ obtained for the reactive bilayer under 25 V, the predicted H_{final} is 391 nm. This is very close to the observed height (∼400 nm). The predicted H_{final} for the same reactive bilayer under 37 V ($D/\langle d \rangle = 0.78$) is 450 nm, which is also similar to the observed height (∼420 nm). This simple calculation suggests that the pillars in the reactive bilayer did not touch the cured PDMS layer. Therefore, we conclude that the flatness of the top of the pillars as well as the smaller height of the pillars observed in the reactive bilayer employed in this study is mainly due to the formation of Y-shaped graft copolymers. This is because a rather flat top of the pillars was observed even at earlier times and higher interfacial strength resulting from the larger interfacial area generation by graft copolymers compared with that by diblock copolymers.[34]

V. Conclusions

In this study, we have shown that λ_{max} as well as pillar sizes of a reactive bilayer consisting of (PS + PS-mCOOH) and PMMA-GMA decreased with increasing amounts of PS-mCOOH because of the reduction of interfacial tension from the formation of in-situ PMMA-*g*-PS copolymer. We found that the prediction of $\lambda_{max} \sim \gamma^{1/2}$ holds for reactive bilayer. The interfacial tension reduction obtained from λ_{max} was consistent with dispersed domain size reduction with increasing amount of PS-mCOOH. But, the height of PMMA-GMA pillars was smaller compared with that in a nonreactive blend. Also, these pillars did not touch the cured PDMS layer and have a flattened top surface. The smaller height of

the pillars compared with the nonreactive bilayer is not due to the mobility resulting from in-situ formed copolymer or insufficient E-field. Rather, it is due to the Y-shaped graft copolymers formed in-situ at the interface. We found that the development of pillar growth of a reactive blend was greatly influenced by the chain architecture of in-situ formed copolymers at the interface.

Acknowledgment. We appreciated the constructive comments made by anonymous reviewers. This work was supported by the National Creative Research Initiative Program supported by KOSEF and by Korea Research Foundation (KRF-20020005-D0008).

References and Notes

(1) Killat, U. *J. Appl. Phys.* **1975**, *46*, 5169.
(2) Onuki, A. *Physica A* **1995**, *217*, 38.
(3) Herminghaus, S. *Phys. Rev. Lett.* **1999**, *83*, 2359.
(4) Taylor, G. I.; McEwan, A. D. *J. Fluid Mech.* **1965**, *22*, 1.
(5) Devitt, E. B.; Melcher, J. R. *Phys. Fluids* **1965**, *8*, 1193.
(6) Reynolds, J. M. *Phys. Fluids* **1965**, *8*, 161.
(7) Oddershede, L.; Nagel, S. R. *Phys. Rev. Lett.* **2000**, *85*, 1234.
(8) Amundson, K.; Helfand, E.; Quan, X.; Hudson, S. D.; Smith, S. D. *Macromolecules* **1994**, *27*, 6559.
(9) Markved, T. L.; Lu, M.; Urbas, A. M.; Ehrichs, E. E.; Jaeger, H. M.; Mansky, P.; Russell, T. P. *Science* **1996**, *273*, 931.
(10) Thurn-Albrecht, T.; DeRouchey, J.; Russell, T. P.; Jaeger, H. M. *Macromolecules* **2000**, *33*, 3250.
(11) Böker, A.; Elbs, H.; Hänsel, H.; Knoll, A.; Ludwigs, S.; Zettl, H.; Zvelindovsky, A. V.; Sevink, G. J. A.; Urban, V.; Abetz, V.; Müller, A. H. E.; Krausch, G. *Macromolecules* **2003**, *36*, 8078.
(12) Schäffer, E.; Thurn-Albercht, T.; Russell, T. P.; Steiner, U. *Nature (London)* **2000**, *403*, 874.
(13) Schäffer, E.; Thurn-Albercht, T.; Russell, T. P.; Steiner, U. *Europhys. Lett.* **2001**, *53*, 518.
(14) Lin, Z.; Kerle, T.; Baker, S. M.; Hoagland, D. A.; Schaffer, E.; Steiner, U.; Russell, T. P. *J. Chem. Phys.* **2001**, *114*, 2377.
(15) Lin, Z.; Kerle, T.; Russell, T. P.; Schaffer, E.; Steiner, U. *Macromolecules* **2002**, *35*, 3971.
(16) Lin, Z.; Kerle, T.; Russell, T. P.; Schaffer, E.; Steiner, U. *Macromolecules* **2002**, *35*, 6255.
(17) Morariu, M. D.; Voicu, N. E.; Schäffer, E.; Lin, Z.; Russell, T. P.; Steiner, U. *Nat. Mater.* **2003**, *2*, 48.
(18) Pease, L. F., III; Russel, W. B. *Langmuir* **2004**, *20*, 795; *J. Chem. Phys.* **2003**, *118*, 3790; *J. Non-Newtonian Fluid Mech.* **2002**, *102*, 233.
(19) Anastasiadis, S. H.; Gancarz, I.; Koberstein, J. T. *Macromolecules* **1989**, *22*, 1449.
(20) Budkowski, A.; Klein, J.; Steiner, U.; Fetters, L. J. *Macromolecules* **1993**, *26*, 2470.
(21) Macosko, C. W.; Guegan, P.; Khandpur, A. K.; Nakayama, A.; Marechal, P.; Inoue, T. *Macromolecules* **1996**, *29*, 5590.
(22) Kim, J. K.; Lee, H. *Polymer* **1996**, *37*, 305.
(23) Jeon, H. K.; Kim, J. K. *Polymer* **1998**, *39*, 6227; *Korea Polym. J.* **1999**, *7*, 124.
(24) Jeon, H. K.; Kim, J. K. *Macromolecules* **1998**, *31*, 9273; *Macromolecules* **2000**, *33*, 8200.
(25) Jeon, H. K.; O, H. T.; Kim, J. K. *Polymer* **2001**, *42*, 3259.
(26) Schulze, J. S.; Moon, B.; Lodge, T. P.; Macosko, C. W. *Macromolecules* **2001**, *34*, 200.
(27) Kim, H. Y.; Jeong, U.; Kim, J. K. *Macromolecules* **2003**, *36*, 1594.
(28) Kim, J. K.; Jeong, W. Y.; Son, J. M.; Jeon, H. K. *Macromolecules* **2000**, *33*, 9161.
(29) Kim, J. K.; Kim, S.; Park, C. E. *Polymer* **1997**, *38*, 2155.
(30) Wu, S. *Polym. Eng. Sci.* **1987**, *27*, 335.
(31) Favis, B. D. *Polymer* **1994**, *35*, 1532.
(32) Charoensirisomboon, P.; Inoue, T.; Weber, M. *Polymer* **2000**, *41*, 6907, 4483.
(33) Pan, L.; Chiba, T.; Inoue, T. *Polymer* **2001**, *42*, 8825.
(34) Kim, H. Y.; Ryu, D. Y.; Jeong, U.; Kho, D. H.; Kim, J. K. Submitted for publication.
(35) James, E. M., Ed. *Polymer Data Handbook*; Oxford University Press: New York, 1999.

MA0495846